Fluid Phase Equilibria 311 (2011) 67–75

Contents lists available at SciVerse ScienceDirect

Fluid Phase Equilibria

journal homepage: www.elsevier.com/locate/fluid

Thermodynamic modeling for CO_2 absorption in aqueous MEA solution with electrolyte NRTL model

Ying Zhang [a], Huiling Que [a], Chau-Chyun Chen [b,*]

[a] AspenTech Limited, Pudong, Shanghai 201203, China
[b] Aspen Technology, Inc., Burlington, MA 01803, USA

ARTICLE INFO

Article history:
Received 8 April 2011
Received in revised form 16 July 2011
Accepted 27 August 2011
Available online 3 September 2011

Keywords:
Electrolyte NRTL model
Vapor–liquid equilibrium
CO_2 absorption
Monoethanolamine
Enthalpy of absorption
Activity coefficient

ABSTRACT

Accurate modeling of thermodynamic properties of CO_2 absorption in aqueous alkanolamine solutions is essential for simulation and design of such CO_2 capture processes. In this study, we use the Electrolyte Nonrandom Two-liquid activity coefficient model in Aspen Plus to develop a rigorous and thermodynamically consistent representation for the MEA–H_2O–CO_2 system. Vapor–liquid equilibrium (VLE), heat capacity and excess enthalpy data for the binary aqueous amine system (MEA–H_2O) are used to determine the NRTL interaction parameters for the MEA–H_2O binary. VLE, enthalpy of absorption, heat capacity and NMR spectroscopic data for the MEA–H_2O–CO_2 ternary system are used to identify the electrolyte NRTL interaction parameters for the molecule–electrolyte binaries and the previously unavailable standard state properties of the amine ions, MEA protonate and carbamate. The predicted VLE, enthalpy of absorption, heat capacity and speciation for the MEA–H_2O–CO_2 system are compared favorably to experimental data.

1. Introduction

For many decades aqueous monoethanolamine (MEA) solution has been widely used in the absorption/stripping operations for acid gas removal [1]. The recent interest in CO_2 capture with amines has further increased attention on the MEA solution. To properly simulate and design the CO_2 absorption/stripping processes with the aqueous MEA solutions, it is essential to understand the process fundamentals. Knowledge of vapor–liquid equilibrium is the basis for the simulation and design of acid gas absorption/stripping processes [2]. In addition, mass transfer rate-based simulation models requires knowledge on liquid phase speciation resulting from aqueous phase reactions [3]. Furthermore, to evaluate and optimize energy consumption for CO_2 capture, accurate knowledge on the enthalpy of CO_2 absorption is essential. In other words, scalable simulation, design and optimization of the CO_2 capture processes start with the modeling of thermodynamic properties, specifically vapor–liquid equilibrium, chemical reaction equilibrium, as well as calorimetric properties.

Excess Gibbs energy-based activity coefficient models provide a practical and rigorous thermodynamic framework to model thermodynamic properties of aqueous electrolyte systems including aqueous alkanolamines systems for CO_2 capture [4,5]. For example, Austgen et al. [2] and Posey [6] applied electrolyte NRTL model [7–9] to correlate CO_2 solubilities in aqueous MEA solution and other aqueous alkanolamines. Hilliard [10] updated these MEA modeling studies and fitted the VLE, enthalpy of absorption, heat capacity and speciation data from NMR spectrum. Faramarzi et al. [11] used the extended UNIQUAC model [12] to represent VLE for CO_2 absorption in aqueous MDEA, MEA and mixtures of the two alkanolamines. They also predicted concentrations of the species in both MDEA and MEA solutions containing CO_2 and in the case of MEA compared to NMR spectroscopic measurements [10,13]. Recently, Hessen et al. [14] used a refined electrolyte NRTL model [15] to correlate CO_2 solubility in aqueous MEA and MDEA solutions and predict the speciation for the MEA–H_2O–CO_2 and MDEA–H_2O–CO_2 systems.

In this work, we aim to develop an accurate and comprehensive thermodynamic model for CO_2 absorption in aqueous MEA solutions. Specifically we extend our recent work on thermodynamic modeling the MDEA–H_2O–CO_2 system [5], the MDEA–H_2O–CO_2–H_2S system [16], the DIPA–H_2O–CO_2 system, the DIPA–sulfolane–H_2O–CO_2 system, and the MDEA–sulfolane–H_2O–CO_2 system [17]. We use the 2009 version [7] of the electrolyte NRTL model as the thermodynamic framework to correlate available experimental data for CO_2 absorption in aqueous MEA solution. Many of the thermodynamic properties and calorimetric properties data for the MEA–H_2O–CO_2 system have become available in recent years and they cover wider ranges of temperature, pressure, MEA concentration and CO_2 loading.

* Corresponding author. Tel.: +1 781 221 6420; fax: +1 781 221 6410.
E-mail address: chauchyun.chen@aspentech.com (C.-C. Chen).

0378-3812/$ – see front matter © 2011 Elsevier B.V. All rights reserved.
doi:10.1016/j.fluid.2011.08.025

Table 1
Parameters for PC-SAFT equation of state.

	m	ε	σ	ε^{AB}	k^{AB}	Source
MEA	2.9029	306.20	3.1067	2369.0	0.01903	This work

m, segment number parameter; ε, segment energy parameter (K); σ, segment size parameter (Å); ε^{AB}, association energy parameter (K); k^{AB}, effective association volume parameter (Å^3).

Table 2
Parameters for the standard states properties.

Property	$\Delta_f G^{ig}_{298.15}$ (J/kmol)	$\Delta_f H^{ig}_{298.15}$ (J/kmol)	$\Delta_f G^{\infty,aq}_{298.15}$ (J/kmol)	$\Delta_f H^{\infty,aq}_{298.15}$ (J/kmol)	Source
MEA	-1.0330×10^8	-2.0670×10^8			Aspen Databank [23]
$MEAH^+$			-1.8992×10^8[a]	-3.3442×10^8[a]	This work
$MEACOO^-$			-4.8994×10^8[a]	-6.9313×10^8[a]	This work

[a] The values of $MEAH^+$ are calculated from the chemical equilibrium constant in Hamborg and Versteeg [20]. The values of $MEACOO^-$ are calculated from the chemical equilibrium constant in Kim et al. [21]. They are used as the initial guess to fit the experimental data.

Table 3
Parameters for ideal gas heat capacity.[a]

	Unit	C_{1i}	C_{2i}	C_{3i}	C_{4i}	Source
MEA	J/kmol K	1.3207×10^4	2.8158×10^2	-0.1513	3.1287×10^{-5}	Aspen Databank [23]

[a] Correlation for the ideal gas heat capacity, $C^{ig}_p = C_{1i} + C_{2i}T + C_{3i}T^2 + C_{4i}T^3$, $283 < T < 1000$, The unit for temperature is K.

The binary NRTL parameters for MEA–water binary are regressed from the binary VLE, excess enthalpy and heat capacity data. The binary electrolyte NRTL parameters for water–electrolyte binaries and the standard state properties of protonated MEA ion and MEA carbamate are obtained by fitting to the ternary VLE, enthalpy of absorption, heat capacity and NMR spectroscopic data. This updated model for the MEA–H_2O–CO_2 system should cover broader range of conditions and give more reliable predictions over previous works.

In conjunction with use of the electrolyte NRTL model for the liquid phase activity coefficients, we use the PC-SAFT [18,19] equation of state (EOS) for the vapor phase fugacity coefficients. PC-SAFT EOS is chosen over typical cubic EOS because of its ability to model accurately vapor phase fugacity coefficients at high pressures, an important consideration for CO_2 capture and compression. The PC-SAFT parameters for H_2O and CO_2 are taken from our previous work for the MDEA–H_2O–CO_2 system [5]. The parameters for MEA, summarized in Table 1, are obtained from regression of experimental data on vapor pressure, enthalpy of vaporization, liquid heat capacity and liquid density. All the PC-SAFT binary interaction parameters are set to 0.

2. Thermodynamic framework

2.1. Aqueous phase chemical equilibrium

The acid gas solubility in aqueous amines solutions is determined by both its physical solubility and the chemical equilibrium for the aqueous phase reactions among acid gas, water and amines.

Aqueous phase chemical reactions involved in the MEA–H_2O–CO_2 system can be expressed as:

$$2H_2O \leftrightarrow H_3O^+ + OH^- \quad (1)$$

$$MEAH^+ + H_2O \leftrightarrow MEA + H_3O^+ \quad (2)$$

$$MEACOO^- + H_2O \leftrightarrow MEA + HCO_3^- \quad (3)$$

$$CO_2 + 2H_2O \leftrightarrow H_3O^+ + HCO_3^- \quad (4)$$

$$HCO_3^- + H_2O \leftrightarrow H_3O^+ + CO_3^{-2} \quad (5)$$

We calculate chemical equilibrium constants from the reference state Gibbs free energies of the participating components

$$-RT \ \ln \ K_j = \Delta G^\circ_j \quad (6)$$

where K_j is the chemical equilibrium constant of reaction j, ΔG°_j is the reference state Gibbs energy change for reaction j, R is the universal gas constant, and T is the system temperature.

For the aqueous phase reactions, the reference states chosen are pure liquid for the solvents water and MEA and aqueous phase infinite dilution for the solutes, ionic and molecular.

The calculation method for the Gibbs energies of the solvents and solutes together with the standard state property constants have been summarized in our previous work [5]. Additional standard state property constants for MEA, $MEAH^+$, and $MEACOO^-$ are given in Tables 2–4. We calculate the standard state properties of $MEAH^+$ ion from the experimental chemical equilibrium constant of Eq. (2), as reported by Hamborg and Versteeg [20]. Likewise, we calculate those of $MEACOO^-$ ion from the chemical equilibrium constant of Eq. (3), as reported by Kim et al. [21] These calculated standard state properties for $MEAH^+$ and $MEACOO^-$ are then used as part of the adjustable parameters in fitting the experimental data of thermodynamic properties.

2.2. Physical solubility

Physical solubility is the equilibrium between gaseous CO_2 molecules and CO_2 molecules in the aqueous amine solutions. It can be expressed by Henry's law:

$$P \cdot y_{CO_2} \cdot \phi_{CO_2} = H_{CO_2} \cdot x_{CO_2} \cdot \gamma^*_{CO_2} \quad (7)$$

Table 4
Parameters for aqueous phase infinite dilution heat capacity.[a]

	$MEAH^+$ (J/kmol K)	$MEACOO^-$ (J/kmol K)
Source	This work	This work
$C^{\infty,aq}_{p,i}$	1.82×10^5	-1.80×10^5

[a] The $C^{\infty,aq}_{p,i}$ values of $MEAH^+$ and $MEACOO^-$ are calculated from the chemical equilibrium constants in Hamborg and Versteeg [20] and Kim et al. [21], which are used as the initial guess to fit experimental data.

Table 5
Parameters for dielectric constant.[a]

	A_i	B_i	C_i	Source
MEA	37.72	0	298.15	Aspen Databank [23]

[a] Correlation for the dielectric constant, $\varepsilon_i(T) = A_i + B_i((1/T) - (1/C_i))$. The unit for temperature is K.

where P is the system pressure, y_{CO_2} is the CO_2 mole fraction in vapor phase, ϕ_{CO_2} is the CO_2 fugacity coefficient in vapor phase, H_{CO_2} is the Henry's law constant of CO_2 in the mixed solvent of water and amine, x_{CO_2} is the CO_2 mole fraction in liquid phase, $\gamma^*_{CO_2}$ is the unsymmetric activity coefficient of CO_2 in the mixed solvent of water and amine.

The Henry's constant in the mixed solvent is calculated from those in the pure solvents:

$$\ln\left(\frac{H_i}{\gamma_i^\infty}\right) = \sum_A w_A \ln\left(\frac{H_{iA}}{\gamma_{iA}^\infty}\right) \quad (8)$$

where H_i is the Henry's constant of molecular solute i, i.e., CO_2, in the mixed solvent, H_{iA} is the Henry's constant of molecular solute i in pure solvent A, γ_i^∞ is the infinite dilution activity coefficient of molecular solute i in the mixed solvent, γ_{iA}^∞ is the infinite dilution activity coefficient of molecular solute i in pure solvent A.

Weighting factor w_A is calculated by Eq. (9)

$$w_A = \frac{x_A (V_{iA}^\infty)^{2/3}}{\sum_B x_B (V_{iB}^\infty)^{2/3}} \quad (9)$$

where x_A is the mole fraction of solvent A on solute-free basis, V_{iA}^∞ is the partial molar volume of molecular solute i at infinite dilution in pure solvent A. V_{iA}^∞ is calculated from the Brelvi-O'Connell model [22] with the characteristic volume for the solute ($V_{CO_2}^{BO}$) and solvent (V_s^{BO}). We use the critical volume from Aspen Databank [23], 0.225 m^3/kmol, as the characteristic volume for MEA. $V_{CO_2}^{BO}$ and $V_{H_2O}^{BO}$ can be found in our previous work [5].

The Henry's law constants for CO_2 with water and with MEA are required. The former has been well studied [24] while the knowledge about the latter is relatively limited. The concept of N_2O analogy used to determine the Henry's constant for CO_2 with amine has been summarized previously [5]. Based on the works of Wang et al. [25] and Versteeg and van Swaaij [26], we obtain the following expression for the Henry's constant for CO_2 with MEA:

$$H_{CO_2,MEA} \text{ (Pa)} = 6.6434 \times 10^8 \exp\left(\frac{-896.5}{T}\right) \quad (10)$$

2.3. Enthalpy of absorption

Enthalpy of CO_2 absorption in aqueous MEA solution can be derived from enthalpy balance of the absorption process:

$$\Delta H_{abs} = \frac{n_{Final} H^l_{Final} - n_{Initial} H^l_{Initial} - n_{CO_2} H^v_{CO_2}}{n_{CO_2}} \quad (11)$$

where ΔH_{abs} is the enthalpy of absorption per unit mole of CO_2, H^l_{Final} is the molar enthalpy of the final solution, $H^l_{Initial}$ is the molar enthalpy of the initial solution, $H^v_{CO_2}$ is the molar enthalpy of gaseous CO_2 absorbed, n_{Final} is the number of moles of the final solution, $n_{Initial}$ is the number of moles of the initial solution, n_{CO_2} is the number of moles of CO_2 absorbed.

There are two kinds of enthalpy of absorption, i.e. the integral enthalpy of absorption and the differential enthalpy of absorption. The integral enthalpy of absorption for a certain amine–H_2O–CO_2 system is the heat effect per unit mole of CO_2 during the CO_2 loading process with the CO_2 loading increasing from zero to the final value of the amine–H_2O–CO_2 system. The differential enthalpy of absorption for an amine–H_2O–CO_2 system is the heat effect per unit mole of CO_2 when an infinitesimal amount of CO_2 is added into this amine–H_2O–CO_2 system.

2.4. Activity coefficients

Activity coefficients are required in aqueous phase chemical equilibrium calculations, phase equilibrium calculations, enthalpy of absorption, liquid enthalpy and liquid heat capacity calculations. Activity coefficient of a component in a liquid mixture is function of temperature, pressure, mixture composition and choice of reference state. In vapor–liquid equilibrium calculations we use the infinite dilution mixed solvent reference state for molecular solute CO_2 and in aqueous phase chemical equilibrium calculations we choose the infinite dilution aqueous phase reference state for molecular solute CO_2 and all ionic species.

In applying electrolyte NRTL model for activity coefficient calculations, binary NRTL interaction parameters for molecule–molecule binary, molecule–electrolyte binary and electrolyte–electrolyte binary are required. Here electrolytes are defined as pairs of cation and anion. In addition, solvent dielectric constants are needed to facilitate calculations of long-range ion–ion interaction contribution to activity coefficients. Table 5 shows the dielectric constant correlation for MEA.

Unless specified otherwise, all molecule–molecule binary parameters and electrolyte–electrolyte binary parameters are defaulted to zero and all molecule–electrolyte binary parameters are defaulted to (8, −4). The nonrandomness factor, α, is fixed at 0.2. The calculated thermodynamic properties of the electrolyte solution are dominated by the binary NRTL parameters associated with the major species in the system. For the MEA–H_2O–CO_2 system, the binary parameters for the water–MEA binary, the water–($MEAH^+$, HCO_3^-) binary, the water–($MEAH^+$, $MEACOO^-$) binary determine the predicted thermodynamic properties. These binary parameters are in turn to be identified from fitting to available experimental data.

3. Modeling results

Table 6 summarizes the model parameters and how these parameters are identified in this work. Most of the parameters can be obtained from Aspen Plus databank (see Tables 2–5). Other parameters are determined by fitting to the experimental data.

3.1. MEA

Extensive experimental vapor pressure data, enthalpy of vaporization data, liquid heat capacity data and liquid density data are available for MEA. The PC-SAFT parameters of MEA are regressed from the vapor pressure data [27–30] with average relative deviation of 3.9%, enthalpy of vaporization data [31,32] with average relative deviation of 2.8%, liquid heat capacity data [33,34] with average relative deviation of 0.5% and liquid density data [35–37] with average relative deviation of 0.03%. The identified PC-SAFT parameters for MEA are given in Table 1.

Table 6
Model parameters.

Parameters	Component	Source	Data used for regression
PC-SAFT EOS parameters	H_2O	Gross and Sadowski [19]	
	MEA	Regression	Vapor pressure, enthalpy of vaporization, liquid heat capacity and liquid density data of MEA
	CO_2	Aspen Databank [23]	
Antoine equation	MEA	Aspen Databank [23]	
$\Delta_{vap}H$	MEA	Aspen Databank [23]	
Dielectric constant	MEA	Aspen Databank [23]	
Henry's constant	CO_2 in H_2O	Yan and Chen [24]	
	CO_2 in MEA	This work	
NRTL binary parameters	CO_2–H_2O binary	Yan and Chen [24]	
	MEA–H_2O binary	Regression	VLE, excess enthalpy and heat capacity for MEA–H_2O binary
	Molecule–electrolyte binaries	Regression	VLE, excess enthalpy, heat capacity and species concentration from NMR spectra for MEA–H_2O–CO_2
$\Delta_f G^{ig}_{298.15}$, $\Delta_f H^{ig}_{298.15}$, C_p^{ig}	H_2O, MEA, CO_2	Aspen Databank [23]	
$\Delta_f G^{\infty,aq}_{298.15}$, $\Delta_f H^{\infty,aq}_{298.15}$	H_3O^+, OH^-, HCO_3^-, CO_3^{-2}	Aspen Databank [23]	
	$MEAH^+$, $MEACOO^-$	Regression	VLE, excess enthalpy, heat capacity and species concentration from NMR spectra for MEA–H_2O–CO_2
$C_p^{\infty,aq}$	H_3O^+, OH^-	Aspen Databank [23]	
	HCO_3^-, CO_3^{-2}	Zhang and Chen [5]	
	$MEAH^+$, $MEACOO^-$	Regression	VLE, excess enthalpy, heat capacity and species concentration from NMR spectra for MEA–H_2O–CO_2

3.2. MEA–H_2O system

Table 7 summarizes the extensive literature data on VLE [30,38–42], excess enthalpy [6,38,43,44] and heat capacity [34,45,46] of the MEA–H_2O binary system. These data cover the complete MEA–H_2O binary concentration range from room temperature to 443 K. Together all these data are used to identify the NRTL binary parameters including their temperature dependencies for the MEA–H_2O binary system.

The regressed NRTL parameters are summarized in Table 8. The experimental data for the binary MEA–H_2O system are well represented. The average relative deviations between the calculated values and the experimental data are reported in Table 7. Fig. 1 shows the parity plot while Fig. 2 shows the comparison for the experimental total pressure data and the calculated results from the model. Fig. 3 shows the comparison results for the MEA vapor and liquid composition. The rather large deviations of some data points from Cai et al. [40] and Park and Lee [41] in Fig. 1 show up again in Fig. 3 as these data points deviate significantly from the calculated *T*–*X* and *T*–*Y* curves. The excess enthalpy fit is given in Fig. 4. The experimental excess enthalpy data from Touhara

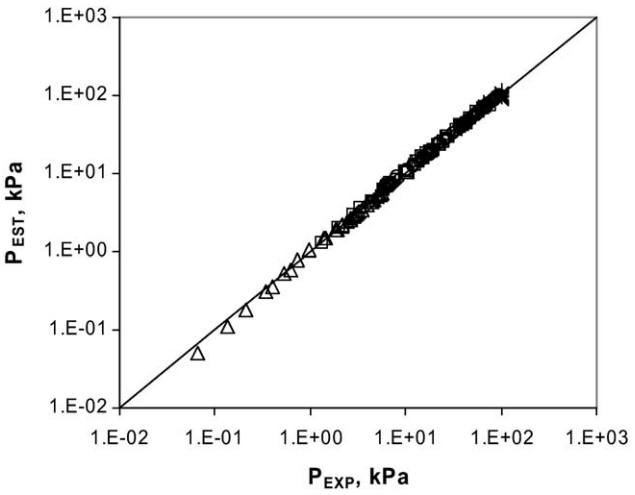

Fig. 1. Parity plot for MEA–H_2O system total pressure: experiment vs. model, (◊) Tochigi et al. [30]; (△) Touhara et al. [38]; (□) Nath and Bender [39]; (+) Cai et al. [40]; (×) Park and Lee [41]; and (○) Kim et al. [42].

Table 7
Experimental data used in the regression for the MEA–H_2O system.

Data type	*T* (K)	Pressure (kPa)	MEA mole fraction	Data points	Average relative deviation, $\lvert\Delta Y/Y\rvert$ (%)	Reference
VLE (isothermal), TPxy	363	4.0–70.1	0–1	11	3.3[a]	Tochigi et al. [30]
VLE (isothermal), TPX	298–308	0.065–5.6	0–1	30	4.2[a]	Touhara et al. [38]
VLE (isothermal), TPX	333–364	1.3–75.8	0–1	41	4.6[a]	Nath and Bender [39]
VLE (isobaric), TPxy	361–443	66.7, 101.3	0–1	29	5.2[a]	Cai et al. [40]
VLE (isobaric), TPxy	373–443	101.3	0–1	18	3.3[a]	Park and Lee [41]
VLE (isothermal), TPxy	313–373	6.1–99.6	0–0.57	87	2.3[a]	Kim et al. [42]
Excess enthalpy (isothermal)	298		0.006–0.98	52	3.3	Touhara et al. [38]
Excess enthalpy (isothermal)	298		0.10–0.95	10	5.3	Buslaeva et al. [43]
Excess enthalpy (isothermal)	298		0.0016–0.0098	5	7.1	Dohnal et al. [44]
Excess enthalpy (isothermal)	298, 342		0.15–0.67	6	2.1	Posey [6]
Heat capacity (isobaric)	303–353		0.2–0.8	44	2.2	Chiu et al. [34]
Heat capacity (isobaric)	283–313		0–1.0	54	2.3	Page et al. [45]
Heat capacity (isobaric)	298		0.10–0.40	4	3.6	Weiland et al. [46]

[a] The average relative deviations are those of total pressure.

Table 8
Regressed NRTL parameters for MEA–H_2O system with $\alpha = 0.2$.[a]

Parameter	Component *i*	Component *j*	Value	Standard deviation
a_{ij}	H_2O	MEA	0.1559	0.4085
a_{ij}	MEA	H_2O	1.5201	0.3234
b_{ij}	H_2O	MEA	110.80	89.04
b_{ij}	MEA	H_2O	−910.30	73.64

[a] Correlation for the NRTL parameters, $\tau_{ij} = a_{ij} + b_{ij}/T$, the unit for temperature is K.

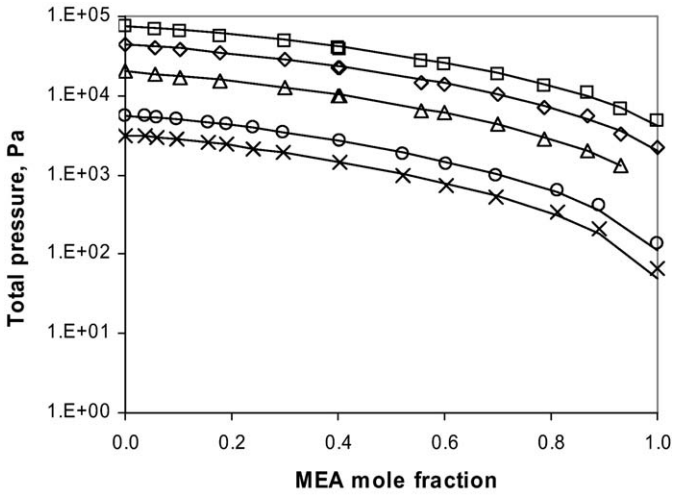

Fig. 2. Comparison of the experimental data (symbols) for the total pressure of MEA–H_2O system and the model results (lines). (×) T = 298 K, Touhara et al. [38]; (○) T = 308 K [38]; (△) T = 333 K, Nath and Bender [39]; (◊) T = 351 K [39]; (□) T = 364 K [39].

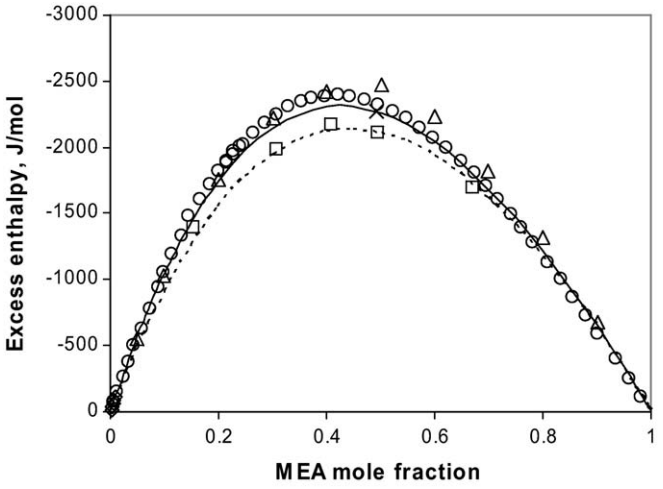

Fig. 4. Comparison of the experimental data (symbols) for the excess enthalpy of MEA–H_2O system and the model results (lines). (○) T = 298 K, Touhara et al. [38]; (△) T = 298 K, Buslaeva et al. [43]; (◊) T = 298 K, Dohnai et al. [44]; (×) T = 298 K, Posey [6]; and (□) T = 342 K [6].

et al. [38], Dohnai et al. [44] and Posey [6] are represented very well. The experimental data of Buslaeva et al. [43] are more negative in value than the others. Fig. 5 shows satisfactory representation of the heat capacity data.

3.3. MEA–H_2O–CO_2 system

Extensive experimental data on VLE [10,47–66], enthalpy of absorption [67], heat capacity [10,46] and NMR spectra [13,68] of the ternary MEA–H_2O–CO_2 system are available. Of particular interesting are the recently released high temperature VLE data of Xu and Rochelle [66] extending the high temperature limit from 423 K to 443 K.

Standard state thermodynamic property parameters ($\Delta_f G^{\infty,aq}_{298.15}$, $\Delta_f H^{\infty,aq}_{298.15}$, and $C_p^{\infty,aq}$) of $MEAH^+$ ion and $MEACOO^-$ ion together with the binary NRTL parameters for major molecule–electrolyte pairs are regressed from selected experimental data of the MEA–H_2O–CO_2 system. Table 9 summarizes the VLE [10,58,65,66], enthalpy of absorption [67], heat capacity [10,46] and species concentration [68] data used to obtain these parameters. The VLE data of Lee et al. [51] are not used because

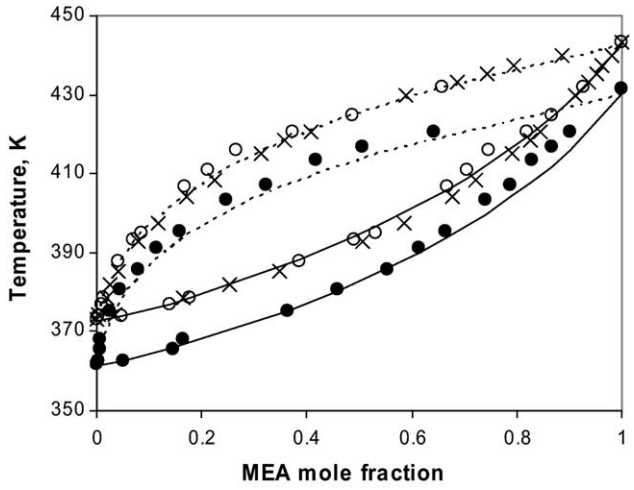

Fig. 3. Comparison of the experimental data (symbols) for the vapor and liquid compositions of MEA–H_2O system and the model results (lines). (○) P = 101 kPa, Cai et al. [40], (●) P = 67 kPa, [40], (×) P = 101 kPa, Park and Lee [41].

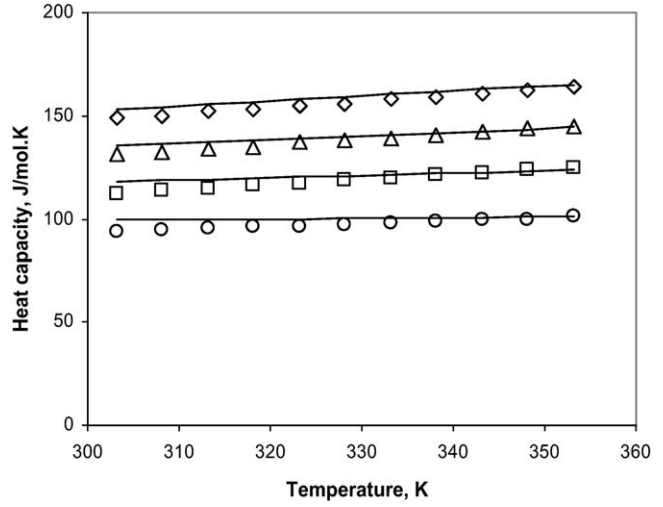

Fig. 5. Comparison of the experimental data from Chiu et al. [34] (symbols) for the heat capacity of MEA–H_2O system and the model results (lines). (○) MEA mole fraction 0.2; (□) MEA mole fraction 0.4; (△) MEA mole fraction 0.6; and (◊) MEA mole fraction 0.8.

Table 9
Experimental data used in the regression for the MEA–H_2O–CO_2 system.

Data type	T (K)	Pressure (kPa)	MEA mole fraction	CO_2 loading	Data points	Average relative deviation $\|\Delta Y/Y\|$, (%)	Reference
VLE, TPxy	313–333	0.005–50	0.06–0.16	0.11–0.59	55	35.5	Hilliard [10]
VLE, TPx, CO_2 pressure	273–423	0.001–20,000	0.11	0.002–1.33	124	33.5	Jou et al. [58]
VLE, TPx, CO_2 pressure	393	7–192	0.11	0.16–0.42	19	13.5	Ma'mun et al. [65]
VLE, TPxy	373–443	12–1626	0.11	0.30–0.52	63	28.0	Xu and Rochelle [66]
Enthalpy of absorption	313–393		0.11	0.04–0.72	84	10.9	Kim and Svendsen [67]
Heat capacity, isobaric	313–393		0.06–0.11	0.10–0.58	102	2.4	Hilliard [10]
Heat capacity, isobaric	298		0.03–0.16	0.05–0.50	20	2.0	Weiland et al. [46]
Species concentration	293–313		0.05–0.11	0.09–0.96	24	35.7	Jakobsen et al. [68]

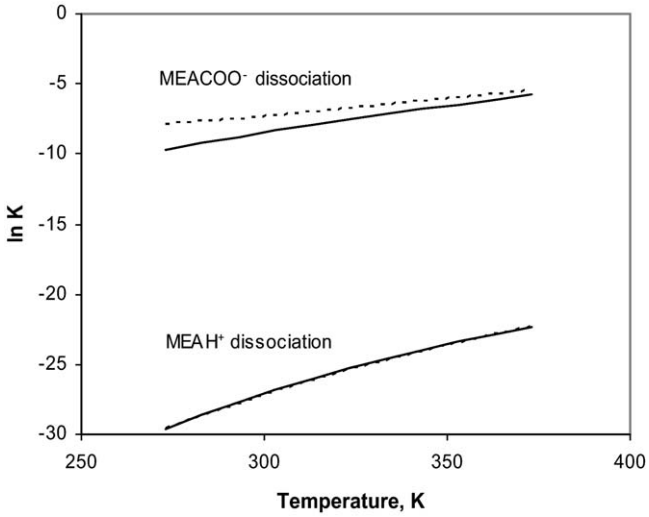

Fig. 6. Comparison of the chemical equilibrium constants from Hamborg and Versteeg [20] for the $MEAH^+$ dissociation reaction and Kim et al. [21] for the $MEACOO^-$ dissociation reaction (–) with those calculated from the regressed $\Delta_f G^{\infty,aq}_{298.15}$, $\Delta_f H^{\infty,aq}_{298.15}$ and $C_p^{\infty,aq}$ parameters (—-).

their measured CO_2 partial pressure data appear to be too low at low CO_2 loading. The speciation data of Böttinger et al. [13] are also excluded because their data lack specific information about the concentrations of MEA, $MEAH^+$ ion and $CO_3{}^{-2}$ ion.

For VLE data, we choose the CO_2 partial pressure data of Jou et al. [58], Ma'mun et al. [65], Hilliard [10] and Xu and Rochelle [66] in the regression. Together these data cover temperature from 273 to 443 K, pressure from 0.001 to 20000 kPa, MEA mole fraction from 0.06 to 0.16 (weight fraction from 0.18 to 0.40) and CO_2 loading from 0.002 to 1.33.

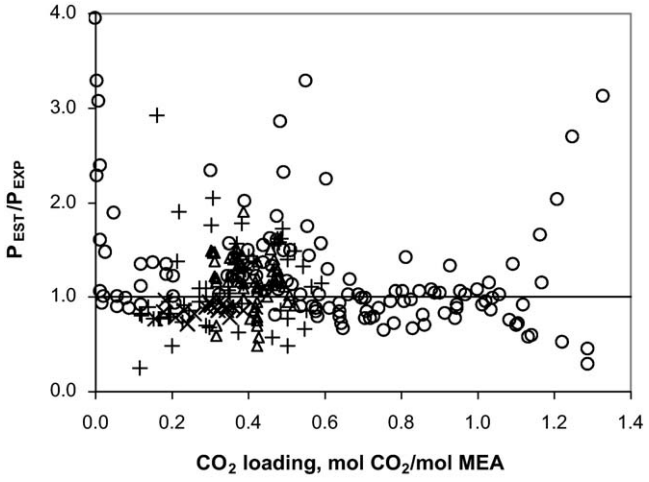

Fig. 7. Ratio of experimental to calculated CO_2 partial pressure as function of CO_2 loading for MEA–H_2O–CO_2 system. (○) Jou et al. [58], (×) Ma'mun et al. [65], (+) Hilliard [10].

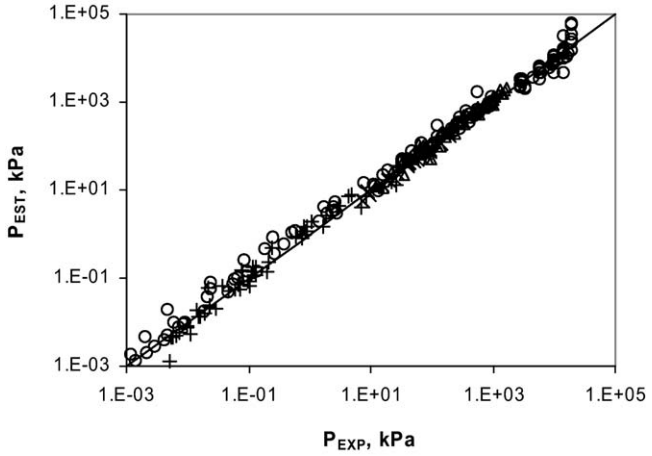

Fig. 8. Parity plot for MEA–H_2O–CO_2 system total pressure: experiment vs. model. (○) Jou et al. [58], (×) Ma'mun et al. [65], and (+) Hilliard [10].

The average relative deviations between the correlation results and the various experimental data are also given in Table 9. The regressed parameters for the MEA–H_2O–CO_2 system are summarized in Table 10. As expected, the regressed values of $\Delta_f G^{\infty,aq}_{298.15}$, $\Delta_f H^{\infty,aq}_{298.15}$ and $C_p^{\infty,aq}$ for $MEAH^+$ ion in Table 10 are comparably close

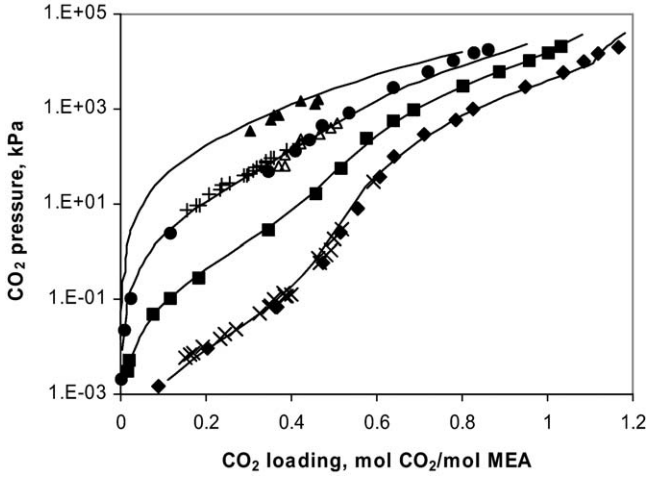

Fig. 9. Comparison of the experimental data (symbols) for CO_2 partial pressure of MEA–H_2O–CO_2 system and the model results (lines), MEA concentration is around 30 wt%. (♦) T = 313 K, Jou et al. [58], (×) T = 313 K, Hilliard [10], (■) T = 353 K, [58], (●) T = 393 K, [58], (+) T = 393 K, Ma'mun et al. [65], (△) T = 393 K, Xu and Rochelle [66], and (▲) T = 433 K, [66].

Table 10
Regressed parameters for MEA–H_2O–CO_2 system with $\alpha = 0.2$.[a]

Parameter	Unit	Component *i*	Component *j*	Value	Standard deviation
$\Delta_f G^{\infty,aq}_{298.15}$	J/kmol	$MEAH^+$		-1.8962×10^8	3.9474×10^5
$\Delta_f H^{\infty,aq}_{298.15}$	J/kmol	$MEAH^+$		-3.3164×10^8	2.7557×10^{10}
$C_p^{\infty,aq}$	J/kmol K	$MEAH^+$		2.1022×10^5	1.0326×10^4
$\Delta_f G^{\infty,aq}_{298.15}$	J/kmol	$MEACOO^-$		-4.9299×10^8	2.7020×10^5
$\Delta_f H^{\infty,aq}_{298.15}$	J/kmol	$MEACOO^-$		-7.0747×10^8	2.7557×10^{10}
$C_p^{\infty,aq}$	J/kmol K	$MEACOO^-$		-4.9781×10^{-2}	5.2297×10^{-1}
a_{ij}		H_2O	($MEAH^+$, $MEACOO^-$)	6.7320	0.4891
a_{ij}		($MEAH^+$, $MEACOO^-$)	H_2O	−3.1628	0.3606
a_{ij}		H_2O	($MEAH^+$, HCO_3^-)	8.5721	0.2403
a_{ij}		($MEAH^+$, HCO_3^-)	H_2O	−4.0092	0.0815
b_{ij}	K	H_2O	($MEAH^+$, $MEACOO^-$)	−9.2407	110.73
b_{ij}	K	($MEAH^+$, $MEACOO^-$)	H_2O	39.498	80.84

[a] Correlation for the NRTL parameters, $\tau_{ij} = a_{ij} + b_{ij}/T$, the unit for temperature is K.

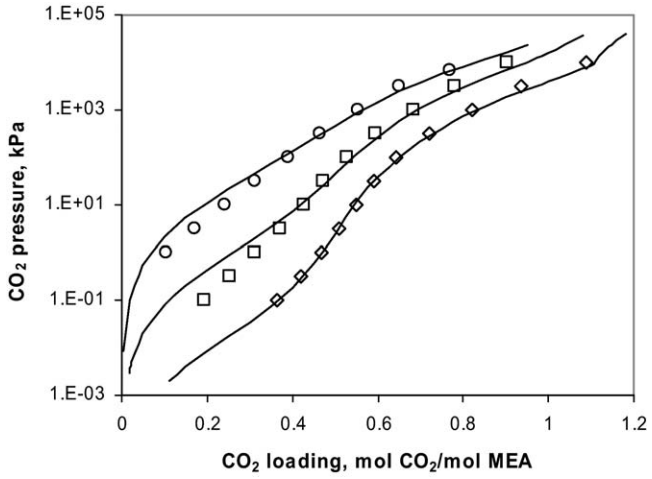

Fig. 10. Comparison of the experimental data (symbols) for CO_2 partial pressure of MEA–H_2O–CO_2 system from Lee et al. [51] and the model results (lines), MEA concentration is around 30 wt%, (◊) $T = 313$ K, (□) $T = 353$ K, and (○) $T = 393$ K.

to the estimated values reported in Tables 2 and 4. The regressed values of $\Delta_f G^{\infty,aq}_{298.15}$ and $\Delta_f H^{\infty,aq}_{298.15}$ for $MEACOO^-$ ion are also close to the estimated values. However, the value of $C_p^{\infty,aq}$ for $MEACOO^-$ ion is more difficult to determine and the result is a small negative value. The chemical equilibrium constants calculated with the

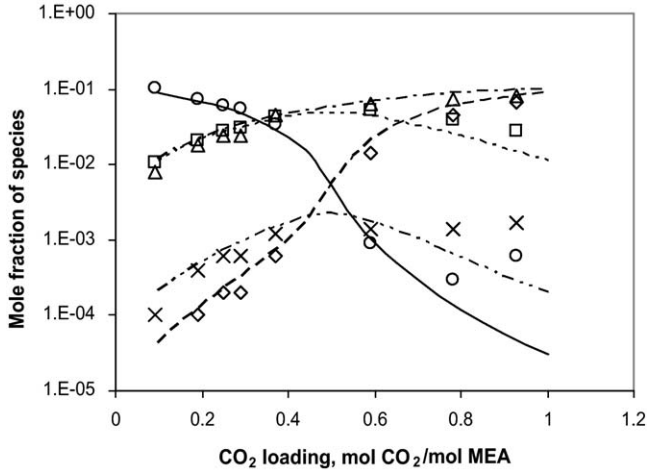

Fig. 11. Comparison of the experimental data (symbols) for species concentration in MEA–H_2O–CO_2 system from Jakobsen et al. [68] and the model results (lines) at $T = 293$ K. MEA concentration is 30 wt%. (○) MEA, (△) $MEAH^+$, (□) $MEACOO^-$, (◊) HCO_3^-, and (×) CO_3^{-2}.

regressed values of $\Delta_f G^{\infty,aq}_{298.15}$, $\Delta_f H^{\infty,aq}_{298.15}$ and $C_p^{\infty,aq}$ are compared with those from the literature [20,21] and shown in Fig. 6. The calculated chemical equilibrium constant for the $MEAH^+$ dissociation reaction (Eq. (2)) is almost identical to those reported by Hamborg and Versteeg [20] while the calculated constant for the $MEACOO^-$ dissociation reaction (Eq. (3)) is slightly higher than those reported by Kim et al. [21].

Figs. 7 and 8 show that most of the CO_2 partial pressure data of Jou et al. [58], Ma'mun et al. [65], Hilliard [10] and Xu and Rochelle [66] are fitted within ±30%. The experimental CO_2 partial pressure data are very well correlated by the model. Fig. 9 shows the satisfactory correlation results for the CO_2 partial pressure data for MEA concentration of 30 wt%, CO_2 loading from 0.003 to 1.20, temperature from 313 to 433 K and pressure up to 20,000 kPa. Fig. 10 further shows that under the same conditions, i.e., $T = 353$ and 393 K, there are systematic deviations between the calculated CO_2 pressures and the experimental data of Lee et al. [51] at low CO_2 loading.

Table 11 shows comparison of the model predictions and the experimental VLE data from numerous other sources not included in the regression. With the exception of the data from Lee et al. [51], Issac et al. [52], Treckmann [54], Song et al. [59], Park et al. [63] and Bonenfant et al. [64], the model predictions are very satisfactory with the average relative deviation on pressure (either total pressure or CO_2 partial pressure) in the range of 28–44%. The results highlight the fact that we cannot match all the VLE data because the experimental data from different sources can be inconsistent.

Fig. 11 shows species distribution as a function of CO_2 loading for a 30 wt% MEA solution at 293 K. The calculated species concentrations are consistent with the experimental NMR measurements from Jakobsen et al. [68].

Figs. 12–14 show comparisons of the model correlations and the experimental data of Kim and Svendsen [67] for the differential enthalpy of CO_2 absorption in aqueous MEA solution at 313, 353 and 393 K, respectively. The calculated values are in reasonable agreement with the experimental data except those at 393 K. Also shown in Figs. 12–14 are the predicted integral enthalpies of CO_2 absorption. The integral enthalpy and the differential enthalpy overlap at low CO_2 loading and then diverge much at high CO_2 loading, i.e., greater than 0.5, where the differential enthalpy drops by more than 50%. We further show the computed differential enthalpy of absorption as sum of the various contributions from reactions 1 to 5, CO_2 dissolution, and excess enthalpy.

$$\Delta H_{\text{abs}} = \sum_{i=1}^{k} \Delta n_i \Delta H_i^{\text{o}} + \Delta H_{\text{dissolution}} + \Delta H^{\text{ex}} \quad (12)$$

where ΔH_{abs} is the differential enthalpy of absorption per mol of CO_2, ΔH_i^{o} is the standard enthalpy of reaction for reaction *i* per mole of key component reacted, Δn_i is the reaction extent of the reaction key component for reaction *i* when one mole CO_2 is absorbed,

Table 11
Comparison between experimental data and model predictions for CO_2 partial pressure of the MEA–H_2O–CO_2 system.

Source	Data points	T (K)	P (kPa)	MEA concentration	CO_2 loading	$\lvert\Delta P/P\rvert$ (%)
Muhlbauer and Monaghan [47]	18	298–373	0.1–140	0.05	0.38–0.74	30.4
Jones et al. [48]	48	313–413	0.08–930	0.05	0.13–0.73	32.2
Lee et al. [49]	45	315–373	1–6600	0.05	0.14–1.19	44.4
Lawson and Garst [50]	24	313–413	3–2800	0.05–0.11	0.11–1.0	30.7
Lee et al. [51]	256	298–393	0.1–10000	0.02–0.11	0.11–2.19	50.5
Isaacs et al. [52]	19	353–373	0.007–1.8	0.05	0.035–0.32	112
Maddox et al. [53]	60	298–353	4–6800	0.05	0.41–1.33	28.6
Treckmann [54]	7	298	5–37	0.02	0.60–0.78	54.1
Austgen et al. [55]	8	313–353	0.1–230	0.05	0.27–0.69	42.6
Shen and Li [56]	13	313	16–2600	0.05	0.56–1.05	35.5
Dawodu and Meisen [57]	5	373	460–3900	0.09	0.54–0.72	43.2
Song et al. [59]	10	313	3–2400	0.11	0.49–1.06	74.4
Jane and Li [60]	7	353	4–120	0.05	0.36–0.58	37.7
Park et al. [61]	7	313	3–2100	0.05	0.51–1.05	28.6
Mathonat et al. [62]	9	313–393	2000–10,000	0.11	0.55–1.67	36.0
Park et al. [63]	13	313	3–2200	0.03–0.05	0.48–1.07	49.8
Bonenfant et al. [64]	2	296	101	0.02	0.81	80.6

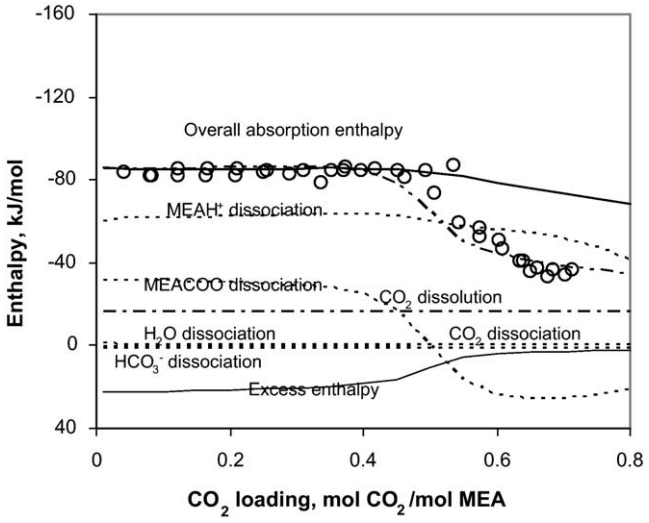

Fig. 12. Differential enthalpy of CO_2 absorption in 30 wt% MEA aqueous solution at 313 K. Symbols (○) represent experimental data from Kim and Svendsen [67]; lines represent model results. (–) integral enthalpy of absorption, (– ·· –) differential enthalpy of solution, (—·) contribution of reactions, (– · –) contribution of CO_2 dissolution, and (– –) contribution of excess enthalpies.

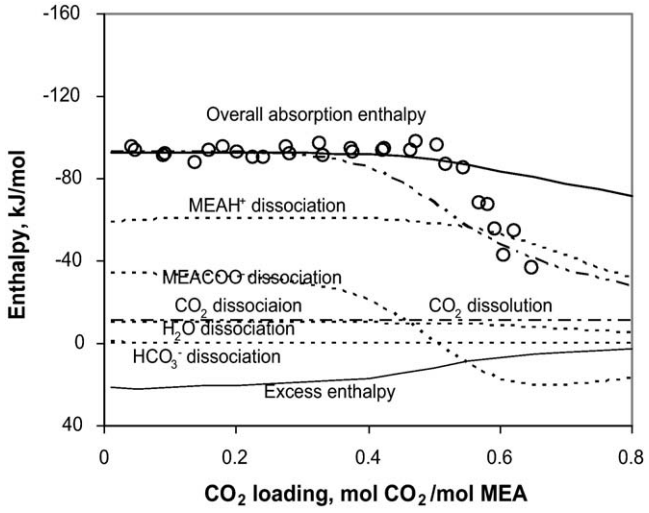

Fig. 13. Differential enthalpy of CO_2 absorption in 30 wt% MEA aqueous solution at 353 K. Symbols (○) represent experimental data from Kim and Svendsen [67]; lines represent model results. (–) integral enthalpy of absorption, (– ·· –) differential enthalpy of solution, (—·) contribution of reactions, (– · –) contribution of CO_2 dissolution, and (– –) contribution of excess enthalpies.

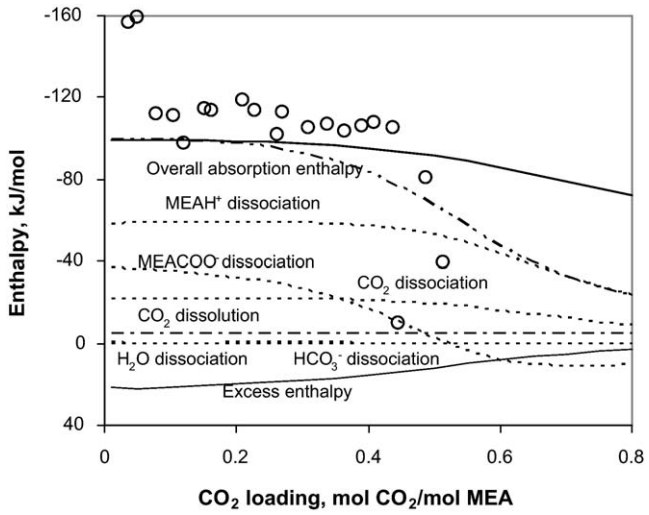

Fig. 14. Differential enthalpy of CO_2 absorption in 30 wt% MEA aqueous solution at 393 K. Symbols (○) represent experimental data from Kim and Svendsen [67]; lines represent model results. (–) integral enthalpy of absorption, (– ·· –) differential enthalpy of solution, (—·) contribution of reactions, (– · –) contribution of CO_2 dissolution, and (– –) contribution of excess enthalpies.

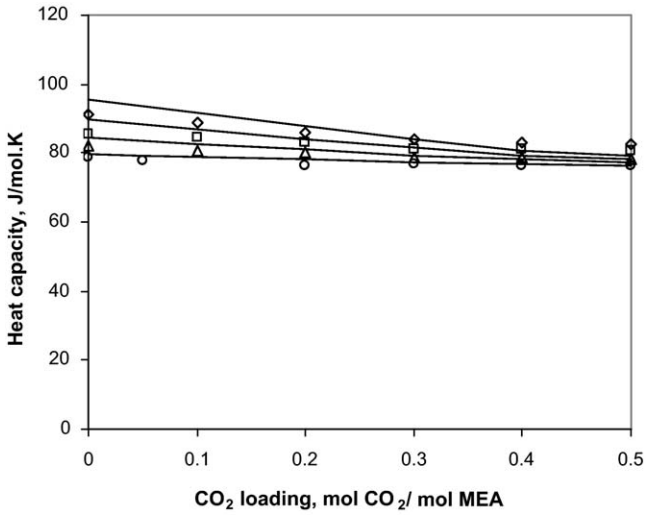

Fig. 15. Comparison of the experimental data (symbols) for heat capacity of MEA–H_2O–CO_2 system from Weiland et al. [46] and the model results (lines) at T = 298 K. (○) 10 wt% MEA, (△) 20 wt% MEA, (□) 30 wt% MEA, and (◊) 40 wt% MEA.

$\Delta H_{dissolution}$ is the enthalpy of CO_2 physical dissolution, ΔH^{ex} is the excess enthalpy.

The results in Figs. 12–14 show that the enthalpy of absorption is dominated by $MEAH^+$ ion and $MEACOO^-$ ion dissociation, and excess enthalpy. In addition, CO_2 dissolution is important around room temperature while CO_2 dissociation becomes more important at higher temperatures.

Fig. 15 shows comparison of the model correlations and the experimental data of Weiland et al. [46] for heat capacity of the MEA–H_2O–CO_2 system. The model results are slightly lower than the experimental data at high loading and high MEA concentration.

4. Conclusion

To support process modeling and simulation of the CO_2 capture process with MEA, the electrolyte NRTL model has been successfully applied to correlate the available data on various thermodynamic properties of the MEA–H_2O–CO_2 system. The model has been validated for predictions of VLE, heat capacity, CO_2 enthalpy of absorption and speciation of the MEA–H_2O–CO_2 system with temperature up to 443 K, pressure up to 20 MPa, MEA concentration up to 40 wt% and CO_2 loading up to 1.33. It should provide a comprehensive thermodynamic representation for the MEA–H_2O–CO_2 system over a broader range of conditions and give more reliable predictions over previous works.

Acknowledgements

The authors thank our colleagues Yuhua Song and Joseph DeVincentis for their reviews and inputs.

References

[1] A.L. Kohl, F.C. Riesenfeld, Gas Purification, 4th ed., Gulf Publishing, Houston, 1985.
[2] D.M. Austgen, G.T. Rochelle, X. Peng, C.-C. Chen, Ind. Eng. Chem. Res. 28 (1989) 1060–1073.
[3] Y. Zhang, H. Chen, C.-C. Chen, J.M. Plaza, R. Dugas, G.T. Rochelle, Ind. Eng. Chem. Res. 48 (2009) 9233–9246.
[4] C.-C. Chen, Fluid Phase Equilib. 241 (2006) 103–112.
[5] Y. Zhang, C.-C. Chen, Ind. Eng. Chem. Res. 50 (2011) 163–175.
[6] M.L. Posey, Thermodynamic Model for Acid Gas Loaded Aqueous Alkanolamine Solutions, PhD thesis, The University of Texas at Austin, 1996.
[7] Y. Song, C.-C. Chen, Ind. Eng. Chem. Res. 48 (2009) 7788–7797.
[8] C.-C. Chen, L.B. Evans, AIChE J. 32 (1986) 444–454.
[9] C.-C. Chen, H.I. Britt, J.F. Boston, L.B. Evans, AIChE J. 28 (1982) 588–596.
[10] M.A. Hilliard, Predictive Thermodynamic Model for an Aqueous Blend of Potassium Carbonate, Piperazine, and Monoethanolamine for Carbon Dioxide, Ph.D. Dissertation, University of Texas at Austin, 2008.
[11] L. Faramarzi, G.M. Kontogeorgis, K. Thomsen, E.H. Stenby, Fluid Phase Equilib. 282 (2009) 121–132.
[12] K. Thomsen, P. Rasmussen, Chem. Eng. Sci. 54 (1999) 1787–1802.
[13] W. Böttinger, M. Maiwald, H. Hasse, Fluid Phase Equilib. 263 (2008) 131–143.
[14] E.T. Hessen, T. Haug-Warberg, H.F. Svendsen, Chem. Eng. Sci. 65 (2010) 3638–3648.
[15] G.M. Bollas, C.-C. Chen, P.I. Barton, AIChE J. 54 (2008) 1608–1624.
[16] Y. Zhang, C.-C. Chen, Ind. Eng. Chem. Res. 50 (2011) 6436–6446.
[17] L. Zong, C.-C. Chen, Fluid Phase Equilib. 306 (2011) 190–203.
[18] J. Gross, G. Sadowski, Ind. Eng. Chem. Res. 40 (2001) 1244–1260.
[19] J. Gross, G. Sadowski, Ind. Eng. Chem. Res. 41 (2002) 5510–5515.
[20] E.S. Hamborg, G.F. Versteeg, J. Chem. Eng. Data 54 (2009) 1318–1328.
[21] I. Kim, K.A. Hoff, E.T. Hessen, T. Haug-Warberg, H.F. Svendsen, Chem. Eng. Sci. 64 (2009) 2027–2038.
[22] S.W. Brelvi, J.P. O'Connell, AIChE J. 18 (1972) 1239–1243.
[23] Aspen Technology Inc., Aspen Physical Property System, v7.2, Burlington, MA, 2010.
[24] Y.-Z. Yan, C.-C. Chen, J Supercrit. Fluids 55 (2010) 623–634.
[25] Y.-W. Wang, S. Xu, F.D. Otto, A.E. Mather, Chem. Eng. J. 48 (1992) 31–40.
[26] G.F. Versteeg, W.P.M. van Swaaij, J. Chem. Eng. Data 33 (1988) 29–34.
[27] J.B. Matthews, J.F. Sumner, E.A. Moelwyn-Hughes, Trans. Faraday Soc. 46 (1950) 797–803.
[28] S.M. Danov, N.B. Mashin, R.V. Efremov, K.K. Slashchinina, Zh. Fiz. Khim. 43 (1969) 733–736.
[29] T.E. Daubert, J.W. Jalowka, V. Goren, AIChE Symp. Ser. 83 (1987) 128–156.
[30] K. Tochigi, K. Akimoto, K. Ochi, F. Liu, Y. Kawase, J. Chem. Eng. Data 44 (1999) 588–590.
[31] G. Liessmann, W. Schmide, S. Reiffarth, Recommended Thermophysical Data. Detherm Database, Dechema e.V.
[32] D. Hopfe, Thermophysical Data of Pure Substances, Detherm Database, Dechema e.V.
[33] Y. Maham, L.G. Hepler, A.E. Mather, A.W. Hakin, R. Marriott, J. Chem. Soc. Faraday Trans. 93 (1997) 1747–1750.
[34] L.-F. Chiu, H.-F. Liu, M.-H. Li, J. Chem. Eng. Data 44 (1999) 631–636.
[35] A. Valtz, C. Coquelet, D. Richon, Thermochim. Acta 428 (2005) 185–191.
[36] J. Aguila-Hernandez, A. Trejo, B.E. Garcia-Flores, R. Molnar, Fluid Phase Equilib. 267 (2008) 172–180.
[37] E. Álvares, F. Cerdeira, D. Gómez-Diaz, J.M. Navaza, J. Chem. Eng. Data 55 (2010) 994–999.
[38] H. Touhara, S. Okazaki, F. Okino, H. Tanaka, K. Ikari, K. Nakanishi, J. Chem. Thermodyn. 14 (1982) 145–156.
[39] A. Nath, E. Bender, J. Chem. Eng. Data 28 (1983) 370–375.
[40] Z. Cai, R. Xie, Z. Wu, J. Chem. Eng. Data 41 (1996) 1101–1103.
[41] S.-B. Park, H. Lee, Korean J. Chem. Eng. 14 (1997) 146–148.
[42] I. Kim, H.F. Svendsen, E. Børresen, J. Chem. Eng. Data 53 (2008) 2521–2531.
[43] M.N. Buslaeva, V.B. Tsvetkov, V.B. Markova, I.F. Kaimin, Koord Khim. 9 (1983) 752–754.
[44] V. Dohnal, A.H. Roux, V. Hynek, J. Solution Chem. 23 (1994) 889–900.
[45] M. Page, J.Y. Huot, C. Jolicoeur, Can. J. Chem. 71 (1993) 1064–1072.
[46] R.H. Weiland, J.C. Dingman, D.B. Cronin, J. Chem. Eng. Data 42 (1997) 1004–1006.
[47] H.G. Muhlbauer, P.R. Monaghan, Oil Gas J. 29 (1957) 139–145.
[48] J.H. Jones, H.R. Froning, E.E. Claytor, J. Chem. Eng. Data 4 (1959) 85–92.
[49] J.I. Lee, F.D. Otto, A.E. Mather, Can. J. Chem. Eng. 52 (1974) 803–805.
[50] J.D. Lawson, A.W. Garst, J. Chem. Eng. Data 21 (1976) 20–30.
[51] J.I. Lee, F.D. Otto, A.E. Mather, J. Appl. Chem. Biotechnol. 26 (1976) 541–549.
[52] E.E. Isaacs, F.D. Otto, A.E. Mather, J. Chem. Eng. Data 25 (1980) 118–120.
[53] R.N. Maddox, A.H. Bhairi, J.R. Diers, P.A. Thomas, Equilibrium Solubility of Carbon Dioxide or Hydrogen Sulfide in Aqueous Solutions of Monoethanolamine Diglycolamine, Diethanolamine and Methyldiethanolamine, 1987, pp. 1–47, GPA Research Report, RR-104.
[54] R. Treckmann, Thermodynamic modelling of the phase equilibrium behavior of H_2S and CO_2 in aqueous solutions of alkanolamines, Diplomarbeit (1987) 1–151.
[55] D.M. Austgen, G.T. Rochelle, C.-C. Chen, Ind. Eng. Chem. Res. 30 (1991) 543–555.
[56] K.-P. Shen, M.-H. Li, J. Chem. Eng. Data 37 (1992) 96–100.
[57] O.F. Dawodu, A. Meisen, J. Chem. Eng. Data 39 (1994) 548–552.
[58] F.-Y. Jou, A.E. Mather, F. Otto, Can. J. Chem. Eng. 73 (1995) 140–147.
[59] J.-H. Song, J.-H. Yoon, H. Lee, K.-H. Lee, J. Chem. Eng. Data 41 (1996) 497–499.
[60] I.-S. Jane, M.-H. Li, J. Chem. Eng. Data 42 (1997) 98–105.
[61] S.-B. Park, C.-S. Shim, H. Lee, K.-H. Lee, Fluid Phase Equilib. 134 (1997) 141–149.
[62] C. Mathonat, V. Majer, A.E. Mather, J.P.E. Grolier, Ind. Eng. Chem. Res. 37 (1998) 4136–4141.
[63] J.-Y. Park, S.J. Yoon, H. Lee, J.-H. Yoon, J.-G. Shim, J.K. Lee, B.-Y. Min, H.-M. Eum, M.C. Kang, Fluid Phase Equilib. 202 (2002) 359–366.
[64] D. Bonenfant, M. Mimeault, R. Hausler, Ind. Eng. Chem. Res. 42 (2003) 3179–3184.
[65] S. Ma'mun, R. Nilsen, H.F. Svendsen, O. Juliussen, J. Chem. Eng. Data 50 (2005) 630–634.
[66] Q. Xu, G. Rochelle, Energy Procedia 4 (2011) 117–124.
[67] I. Kim, H.F. Svendsen, Ind. Eng. Chem. Res. 46 (2007) 5803–5809.
[68] J.P. Jakobsen, J. Krane, H.F. Svendsen, Ind. Eng. Chem. Res. 44 (2005) 9894–9903.